Asian Journal of Chemistry; Vol. 36, No. 11 (2024), 2575-2582

ASIAN JOURNAL OF CHEMISTRY

https://doi.org/10.14233/ajchem.2024.32581

Green Synthesis and Characterization of Hydroxyapatite Nanorods with Enhanced Antibacterial and Anticancer Properties

MUNUSAMY SURESH[1,2], PALANISAMY KARTHIKEYAN[3] and PULLAR VADIVEL[4,*]

[1]Department of Chemistry, Sri Sarada Niketan College of Arts and Science for Women, Salem-636354, India
[2]Department of Chemistry, Periyar University, Salem-636011, India
[3]Department of Chemistry, Government Arts and Science College Idappadi, Salem-637102, India
[4]Department of Chemistry, Salem Sowdeswari College, Salem-636010, India

*Corresponding author: E-mail: vadivelsalem@gmail.com

Received: 26 August 2024; *Accepted*: 12 October 2024; *Published online*: 30 October 2024; AJC-21792

This study reports the microwave synthesis of hydroxyapatite nanorods using *Lantana camara* L. flower extract (LCF-HA) and characterized by FTIR, XRD, TEM and SEM-EDX techniques. The extract coating on the hydroxyapatite nanorods improves the antibacterial efficacy against Gram-positive bacteria. The study also evaluates the mitochondrial membrane potential (MMP), generation of reactive oxygen species (ROS) and capacity to induce apoptosis of LCF-HA. It shows that LCF-HA efficiently inhibits the growth of osteosarcoma cells (MG-63) in a dose-dependent manner. The efficacy of LCF-HA in inducing apoptosis in osteosarcoma cells is established by dual acridine orange/ethidium bromide (AO/EB) fluorescence labelling. Additionally, LCF-HA induces an increase in reactive oxygen species (ROS) generation and a reduction in mitochondrial membrane potential (MMP) levels. The findings indicate that derived LCF-HA has significant anticancer efficacy by inducing apoptosis in osteosarcoma cells through enhanced ROS generation, suggesting that derived LCF-HA may serve as a promising therapeutic target for bone cancer cell lines. Furthermore, the study demostrates excellent compatibility with osteoblast cells, highlighting its potential for bone regeneration applications.

Keywords: Bone regeneration, Cancer, Green synthesis, Hydroxyapatite, Infection.

INTRODUCTION

Cancer, a complex disease, significantly impacts the skeletal system, particularly in cases where it has spread to the bones [1,2]. Primary malignant bone tumours, such as chondrosarcoma, osteosarcoma and Ewing sarcoma, account for nearly 70% of all malignancies in this category. Bone metastasis can cause significant health issues, including pain, increased spinal cord compression, impaired mobility and increased calcium levels and joint dysfunction. Despite advancements in clinical treatments, sarcomas remain lethal due to the presence of tumours in the skeletal system [3].

Traditional cancer therapies have become outdated due to advancements in nanotechnology and multitargeted medication delivery. Nanomedicine, a subdivision of nanotechnologies, employs tailored nanoparticles for the treatment of cancer [4]. This novel strategy has the capacity to detect and control cancer during its first phases, providing outstanding dependability, strong solubility, bioavailability and adaptability, exceeding traditional cancer therapy procedures.

A significant challenge in the biomaterials research is the development of implant coatings that exhibit three crucial characteristics *viz.*, biocompatibility, bioactivity and sufficient mechanical strength. Hydroxyapatite, a vital mineral component of human skeletal system, has great promise for several applications, including drug delivery systems [5,6]. Plant derived extracts are becoming more often used in nanotechnology as a means of environmentally friendly synthesis. Plant extracts with high levels amounts of tannins and polyphenols provide several benefits. They serve as natural additives in food and as agents for the process of tanning leather. Due to their high affinity for metal ions, they are highly suitable for use as reducing, stabilizing and chelating agents in material synthesis [7].

Lantana camara L. (LCF), a member of the Verbenaceae family, is a prevalent invasive plant renowned for its possible medicinal properties. Traditional healers have used LCF extracts for many years to effectively cure a wide range of ailments [8,9]. It is important to recognize that the chemical composition and number of phytochemicals may significantly differ across different species of *Lantana camara* L.

This work demonstrates a novel approach for producing hydroxyapatite nanorods by a sustainable synthesis technique including an extract derived from the flower of *Lantana camara* L. plant (LCF). The use of plant extracts for the production of environmental friendly nanomaterials has significant promise due to their abundant presence of biomolecules like as polyphenols and tannins, which possess the ability to diminish, stabilize and chelate. The study used *L. camara* L. flower extract because of its substantial tannin content. The microwave assisted synthesis approach was selected because to its several advantages, including the capacity to accurately modify the composition, attain high molecular uniformity, reduce crystallization temperatures and produce ultrafine nanorods. This study examines the synthesis and characterization of hydroxyapatite and LCF-HA nanorods, with a specific emphasis on their morphology, antimicrobial efficacy, anticancer activity and compatibility with osteoblast cells.

EXPERIMENTAL

Synthesis of LCF-HA nanorods: High-purity (> 99%) analytical grade $CaCl_2$ and $NH_4H_2PO_4$ were obtained from Sigma-Aldrich and dissolved in deionized water to prepare 1 M $CaCl_2$ and 0.6 M $NH_4H_2PO_4$ solutions, respectively. A 1 M $CaCl_2$ solution was combined with a 0.6 M $NH_4H_2PO_4$ solution and the pH was adjusted to 9 using aqueous NH_3. The *Lantana camara* L. flower (LCF) extract was prepared by boiling the dried LCF in deionized water, followed by filtration and storage at 5 °C. The LCF extract was added to the hydroxyapatite precursor solution and sonicated for 30 min. The mixture was incubated at room temperature for 24 h, resulting in the precipitation. The precipitate was dehydrated using a microwave oven and calcined at 100 °C for 1 h. The dehydrated product was ground to a fine powder to obtain LCF-HA nanorods.

Characterization of LCF-HA nanorods: A Perkin-Elmer Fourier transform spectrometer was utilized to acquire FTIR spectra at room temperature. The phase structure of the prepared samples was analyzed using PAN analytical XRD instrument. The morphology of the prepared samples was examined using SEM (VEGA3, TESCAN) and EDAX equipment. The surface structure and SAED patterns of the synthesized LCF-HA were obtained using the HR-TEM (JEOL JEM 2100).

Cell cultures: MC3T3-E1 cells and osteosarcoma (MG-63) cells were cultured in DMEM medium with 10% FBS, 1% antibiotic (penicillin/streptomycin (PS)) and 1% l-glutamine. The cells were incubated at 37 °C in a 5% CO_2-humidified environment. The cytotoxicity effects of LCF-HA derived the MC3T3-E1 and osteosarcoma cell line were assessed using the MTT assay technique. In brief, the cells were unformly distributed in a 96-well plate at a density of 4×10^6 cells per well in 100 µL of complete media and thereafter subjected to incubation. After 24 h, the LCF-HA was introduced into the cell layer at doses of 10 µg/mL to 100 µg/mL. Following incubation, 50 µL of MTT solution with a concentration of 1 mg/mL was introduced to each well. The cells were then cultured in a light-restricted environment at 37 °C for 4 h. Subsequently, the medium was extracted and the formazan crystals that were produced were dispersed in 100 µL of DMSO. Within a time, frame of 20 min, the absorbance was quantified using a microplate reader that reads at a wavelength of 540 nm. The response percentage for each treatment was calculated by assuming 100% responsiveness in untreated control cells.

$$\text{Viability } (\%) = \frac{\text{Samples absorbance}}{\text{Control absorbance}} \times 100$$

ROS assay: The quantity of reactive oxygen species (ROS) in the cells was measured by quantifying the fluorescence of 2',7'-dichlorofluorescein diacetate (DCFH-DA). The cells were seeded in 12-well plates at a concentration of 3×10^6 and left to incubate overnight. The next day, the medium is substituted with a new medium containing LCF-HA at the concentrations of 30, 50 and 100 µg/mL. Subsequently, the concoction was subjected to incubation at 37 ºC for 1 day. After the period of development, the cells were subjected to protease treatment to separate them from the culture medium and then dyed with DCFH-DA for a length of 15 min. The surplus dye was eliminated *via* washing with a buffer solution. The cells were observed using fluorescence at a wavelength of 540 nm.

Mitochondrial membrane potential assay: Osteosarcoma cells were seeded in a six-well plate and treated with varying concentrations of LCF-HA (30, 50 and 100 µg/mL). After 24 h, cells were washed with a buffer solution, fixed with alcohol and permeabilized with Triton X-100. Cells were incubated with rhodamine-123, a mitochondrial dye and visualized under a fluorescence microscope to assess mitochondrial activity.

Dual staining assay: Dulbecco's modified eagle medium was introduced into each well of a 96-well plate, followed by the addition of cells at a density of 3×10^6/mL and then the dish was incubated. The cells used as controls were not treated, whereas the other cells were exposed to LCF-HA at concentrations of 30, 50 and 100 µg/mL throughout the incubation. Following the culturing process, trypsin was introduced into each well, resulting in the detachment of the cells. The 25 µL suspensions were transferred to glass slides. A double staining solution containing 2 µL of acridine orange (AO) and ethidium bromide (EB) has been added to the solutions and stirred gently for 5 min. The solution was transferred onto a slide and then covered with a coverslip. The shape and size of the cells that underwent apoptosis was examined, whereas the cell number was determined using a fluorescence microscope.

RESULTS AND DISCUSSION

Functional groups analysis: The chemical composition and component interactions are revealed by FTIR spectra (Fig. 1). Both hydroxyapatite (HA) and LCF-HA spectra show distinct bands for water, phosphate, carbonate and hydroxyl indicating

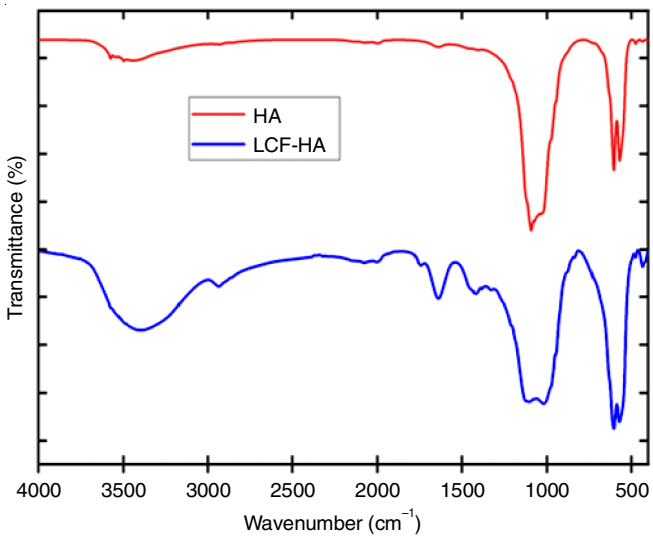

Fig. 1. FTIR spectra of hydroxyapatite (HA) and LCF-HA nanorods

that HA was produced as the predominant phase [10,11]. This observation is crucial since it preserves HA core structure even with the LCF extract. Compared to HA, LCF-HA spectrum exhibits the additional absorption bands. Bands at 3412, 1745, 1419 and 838 cm^{-1} imply the presence of the alcohols, esters and aromatic moieties, respectively. In addition, LCF-HA spectrum also shows a broader band at 3412 cm^{-1} as compared to HA. A broader spectral range may imply an interaction between LCF extract hydroxyl groups and HA surface hydroxide ions. This interaction may increase LCF-HA nanorod surface functionalities, making them more suitable for biological applications.

Phase analysis: X-ray diffraction (XRD) analysis was used to determine the crystal structure of the prepared samples (Fig. 2). The diffraction peaks at 2θ angles of 25°, 31°, 32°, 34° and 41°, confirmed the crytalline nature of HA [12,13]. The XRD pattern of LCF-HA nanoroad showed a modest shift towards lower 2θ values than HA. The inclusion of LCF may have affected the HA phase's lattice properties, as observed by this modification. Interestingly, no further peaks appeared matched to LCF suggesting that it may exist in an amorphous or highly scattered condition inside the LCF-HA nanoroad. Furthermore,

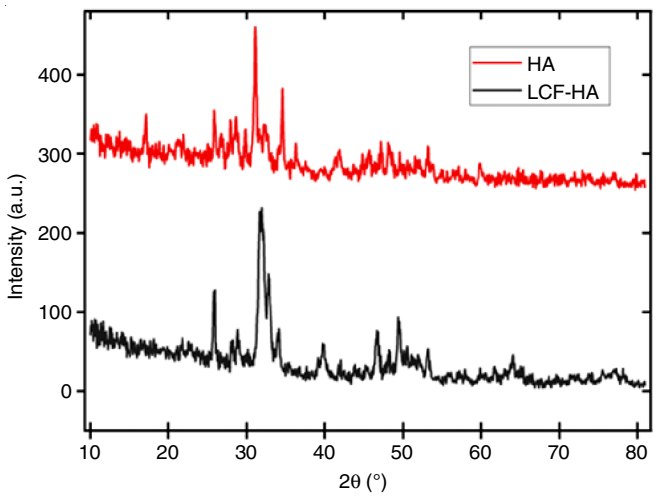

Fig. 2. XRD patterns of hydroxyapatite (HA) and LCF-HA nanorods

the XRD pattern of LCF-HA showed the lower peak intensities than HA, which may be ascribed to a decrease in the crystallinity caused by the addition of LCF (organic extract) and the formation of a nanorod composite structure. All of these findings indicate to the effective development of LCF-HA nanorods composites.

Morphological studies: The scanning electron microscopy (SEM) technique was used to evaluate the morphology of HA and LCF-HA that were produced using microwave irradiation. The HA sample (Fig. 3a) displays non-uniform clusters consisting of elongated crystals. On the other hand, the LCF-HA sample (Fig. 3b) has a clearly distinguishable rod-shaped structure. The nanorod shape is intriguing since it has the potential to increase the biological activity. Previous studies have shown that nanorod-shaped HA has exceptional abilities to combat cancer and bacterial infections [4,14]. The present SEM data are also supported by subsequent transmission electron microscopy (TEM) investigation. These results emphasize the impact of LCF on the structure and shape of HA. The LCF-HA, characterized by its distinctive nanorod structure, emerges as a very intriguing contender for biomedical applications owing to its possibly better biological characteristics. Fig. 3c-d displays the EDAX images for the prepared HA and LCF-HA nanorods. The observation revealed only the peaks for Ca, P and C, signifying the successful formation of the HA and LCF-HA products. Prepared HA and LCF-HA nanorods with a Ca/P molar ratio between 1.68 and 1.70, mimicking the molecular makeup of bones and teeth [15]. The EDAX analysis confirmed that the newly developed nanomaterials are pure.

The TEM images (Fig. 4) showed indistinct nanorod-like structure for HA, but the SAED patterns suggested a well-defined crystalline phase. LCF-HA samples had distinct nanorod shape as observed by TEM, however, the associated SAED patterns indicated a low level of crystallinity. The difference in crystallinity between HA and LCF-HA may be explained by the inclusion of organic materials (LCF) in the hydroxyapatite matrix. Previous research has shown comparable findings, indicating that incorporating organic components into inorganic biomaterials often leads to a decrease in crystallinity [16,17]. Lower crystallinity in HA has been shown to be linked to increased the biological activity, which helps HA imitate real bone more effectively. The findings obtained from TEM-SAED analysis are consistent with the results acquired from FTIR and XRD analysis.

***In vitro* antibacterial activity:** This study investigated the potential of HA and LCF-HA nanorods as antibacterial agents against both Gram-positive (*Staphylococcus aureus*) and Gram-negative (*Escherichia coli*) bacteria, commonly implicated in osteomyelitis (Fig. 5). The agar well-diffusion method revealed a concentration-dependent increase in the zone of inhibition for both HA and LCF-HA. Significantly, the LCF-HA nanorods exhibited significantly greater antibacterial activity compared to HA, particularly against *S. aureus*, a bacterium frequently associated with osteomyelitis. These findings suggest that LCF-HA nanorods hold promise as a novel therapeutic strategy for osteomyelitis. Osteomyelitis is a bone infection characterized by inflammation and potential bone destruction [18]. Current treatment options primarily involve

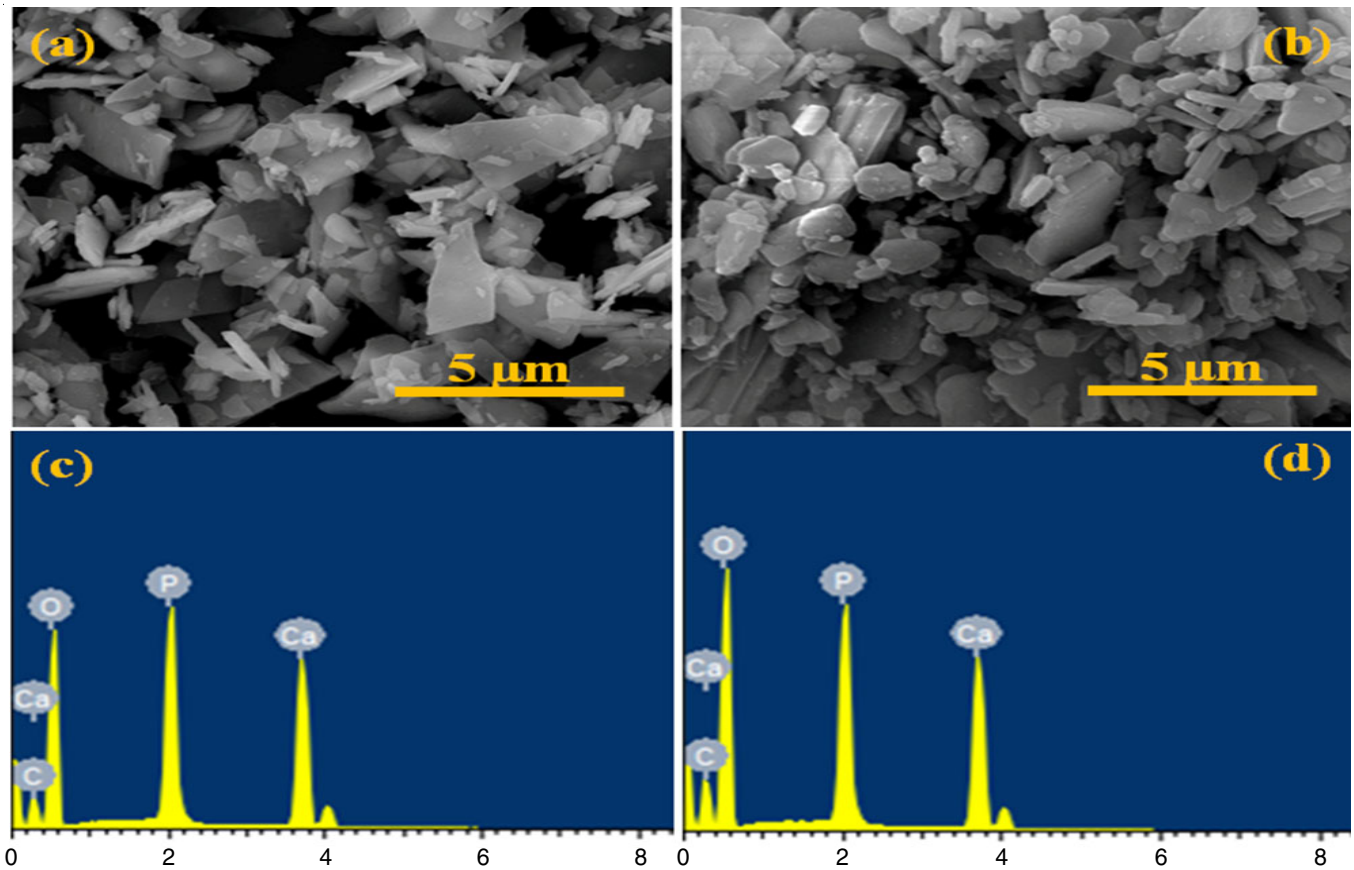

Fig. 3. SEM (a-b) and EDAX (c-d) images of the developed hydroxyapatite (HA) and LCF-HA nanorods

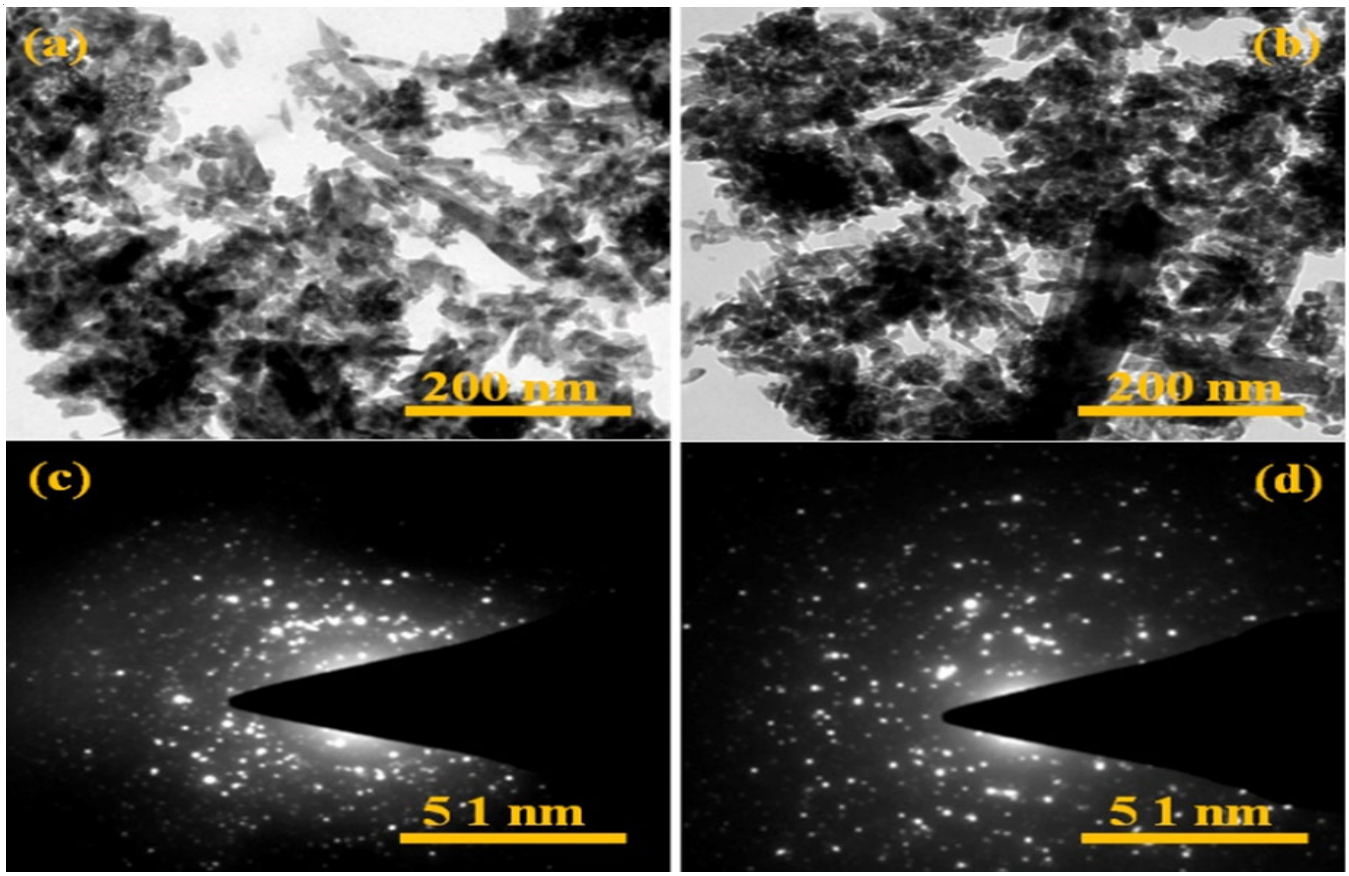

Fig. 4. TEM (a-b) and SAED (c-d) images of the developed hydroxyapatite (HA) and LCF-HA nanorods

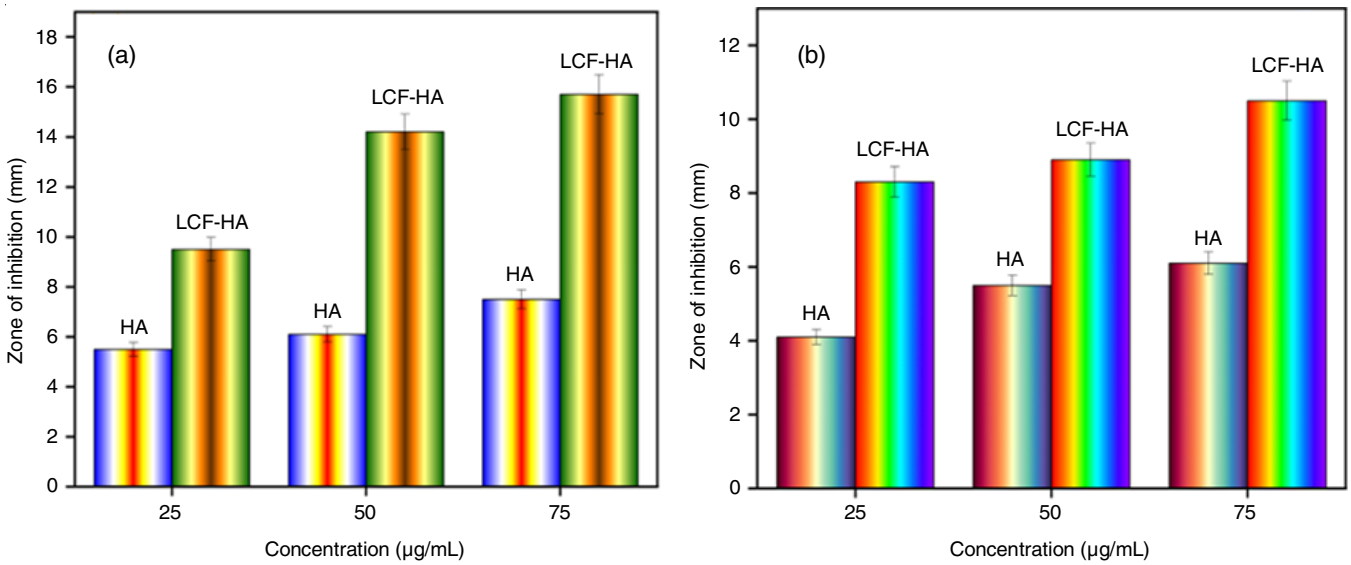

Fig. 5. *In vitro* antibacterials activity of hydroxyapatite (HA) and LCF-HA nanorods against *S. aureus* (a) and *E. coli* bacteria (b)

antibiotic therapy, which can be limited by antibiotic resistance and poor penetration into infected bone tissue. The LCF-HA nanorods, with their superior antibacterial properties, could offer a complementary or alternative approach to combat bacterial infections within the bone microenvironment.

***In vitro* cytocompatibility assay:** Osteosarcoma remains a serious issue despite progress in treatment approaches, mostly because of its resistance to chemotherapy and tendency to recur [19-21]. Therefore, it is crucial to investigate new medicinal materials that have enhanced effectiveness and minimized adverse effects. Within this particular system, this study examined the influence of LCF-HA nanorods on the osteosarcoma cell lines. Osteosarcoma cells (MG-63) were exposed to the different amounts of LCF-HA nanorods for 24 h, ranging from 10 µg/mL to 100 µg/mL. The vitality of the treated cells using the MTT test was also assessed. The research shown that LCF-HA had efficacy in diminishing the survival of cancer cells at different concentrations (30, 50, 70 and 100 µg/mL). Osteosarcoma cells exposed to LCF-HA at concentrations of 30 and 50 µg/mL exhibited the presence of both viable and non-viable cells, as seen in Fig. 6c-d. The cells treated with LCF-HA at a dosage of above 50 µg/mL showed a decrease in the number of viable cells (Fig. 6d-g). The results showed that the LCF-HA nanorods had an inhibitory impact on osteosarcoma cell growth and this effect was dependent on the nanorod dosage. As the concentration of LCF-HA increased, the cancer cells' viability declined,w hich clearly indicate that LCF-HA nanorods have the capacity to inhibit the development and multiplication of osteosarcoma cells.

***In vitro* reactive oxygen species assay:** The study also examined the impact of LCF-HA on osteosarcoma cells by producing reactive oxygen species (ROS). The LCF-HA administration increased the intracellular fluorescence intensity of the ROS-sensitive dye DCFH-DA, indicating a dose-dependent rise in ROS formation (Fig. 7). This suggests that LCF-HA disrupts the cellular redox balance, leading to ROS accumulation, which can damage biological components. Thus, LCF-HA is believed to induce apoptosis in osteosarcoma cells through oxidative stress.

***In vitro* mitochondrial membrane potential:** The study investigated the impact of LCF-HA on mitochondrial activity using the rhodamine 123 dye (Rh-123). The study found that functional mitochondria have a significant mitochondrial membrane potential (ΔΨm), which is crucial for the ATP synthesis.

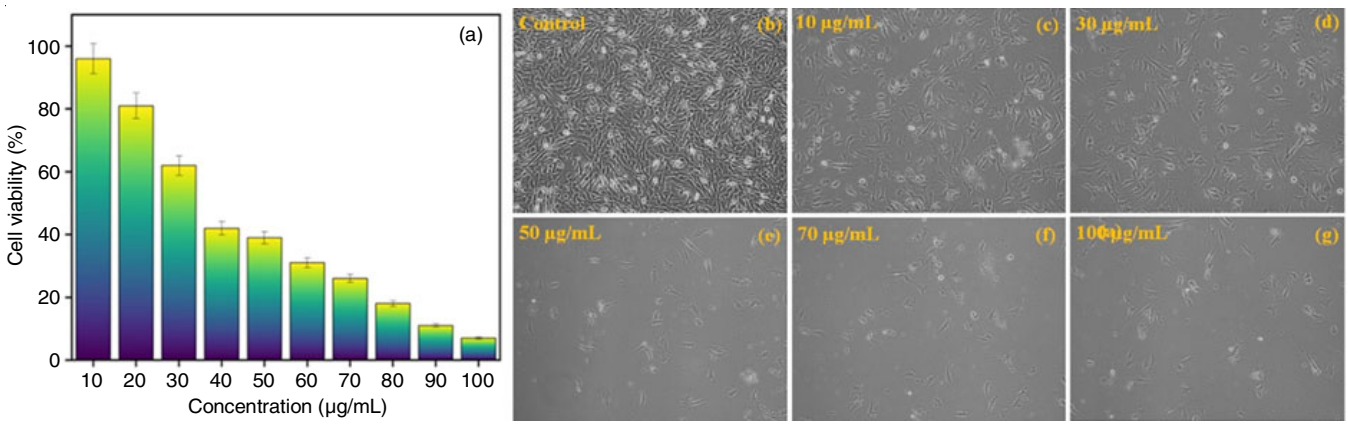

Fig. 6. Cell viability and microscope images of osteosarcoma (MG-63) Cells on LCF-HA nanorods at different concentrations (n = 3)

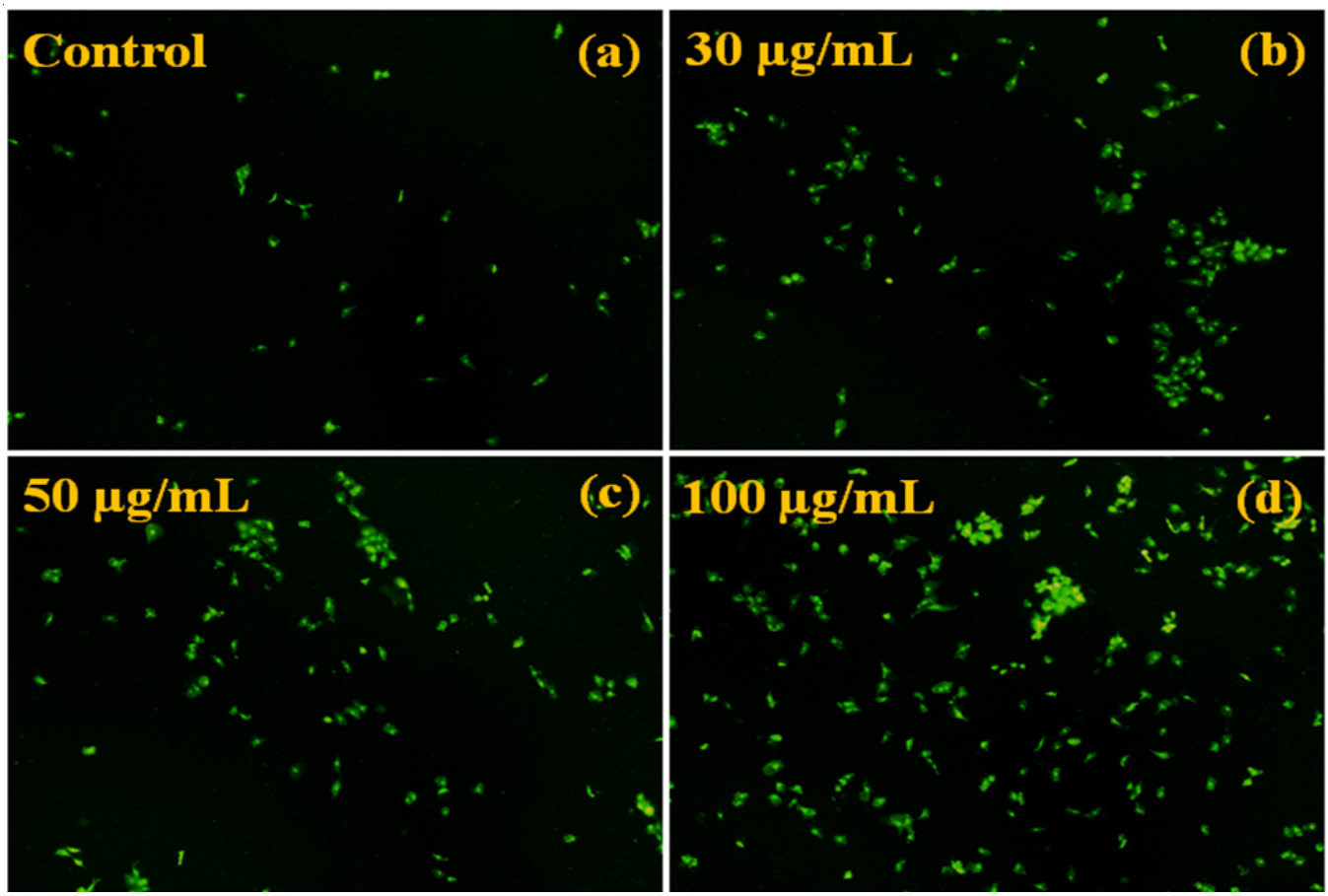

Fig. 7. LCF-HA treatment affected osteosarcoma cells. Lower dose (30 µg/mL) decreased viability, while higher dose (100 µg/mL) increased cell death. A test using DCFH-DA dye confirmed this effect

Rh-123 is taken up by mitochondria in response to changes in ΔΨm, resulting in green fluorescence (Fig. 8). The LCF-HA at doses of 30 and 50 µg/mL showed comparable levels of red fluorescence compared to the control group. However, at 100 µg/mL, a significant reduction in green fluorescence was observed, suggesting a decline in the mitochondrial membrane potential. This is consistent with the reported rise in reactive oxygen species (ROS) generation at this concentration. The findings suggest that LCF-HA may cause a mitochondrial dysfunction-induced apoptotic pathway in osteosarcoma cells when used in greater doses.

***In vitro* apoptosis assay:** The method of staining with acridine orange/ethidium bromide (AO/EB) is often used to detect apoptotic cells by observing their specific morphological alterations [22]. The acridine orange (AO) colours the nucleus to the nucleic acids. During apoptosis, the cell membrane becomes more permeable. Ethidium bromide (EB), a red fluorescent dye, may penetrate the nucleus of apoptotic cells, leading to a distinct orange glow and also selectively attaches to broken DNA, causing this fluorescence. The observed alterations in the present investigation, such as nuclear fragmentation, shrinkage, condensed chromatin and decreased cytoplasm size in cells treated with LCF-HA (Fig. 9b-d), are all characteristic features of apoptosis as determined by AO/EB staining. Early apoptotic cells (30, 50 and 100 µg/mL) may be identified by the presence of more red fluorescence. A treatment with a higher concentration of 100 µg/mL, on the other hand, causes more red fluorescence, which shows that the cells have moved on to late apoptotic stages that are marked by widespread DNA fragmentation. The findings presented here provide evidence that LCF-HA therapy leads to a dose-dependent rise in apoptosis in osteosarcoma cells.

Osteocompatibility: Osteoblasts are the main builders of our skeletal framework [23]. These specialized cells regulate bone formation by synthesizing and mineralizing the extracellular matrix, which acts as the scaffolding that gives bone its shape and strength. They have a crucial impact on the initial development of a strong skeleton throughout infancy and adolescence, as well as the continuous process of bone remodelling. This process involves the continual breakdown and repair of bone tissue, which helps maintain its strength and adapt it to mechanical demands.

The MTT assay was employed to evaluate the influence of LCF-HA on osteoblast viability. As depicted in Fig. 10, LCF-HA exhibited a dose-dependent effect on MC3T3-E1 osteoblast cells. The addition of LCF-HA within the concentration range of 10 to 100 µg/mL significantly enhanced cell survival rates, suggesting its potent proliferative properties. These results align with the therapeutic potential of LCF-HA in bone regeneration. By promoting osteoblast viability and function, the LCF-HA nanorods could accelerate bone healing processes following fractures, surgeries or age-related bone loss.

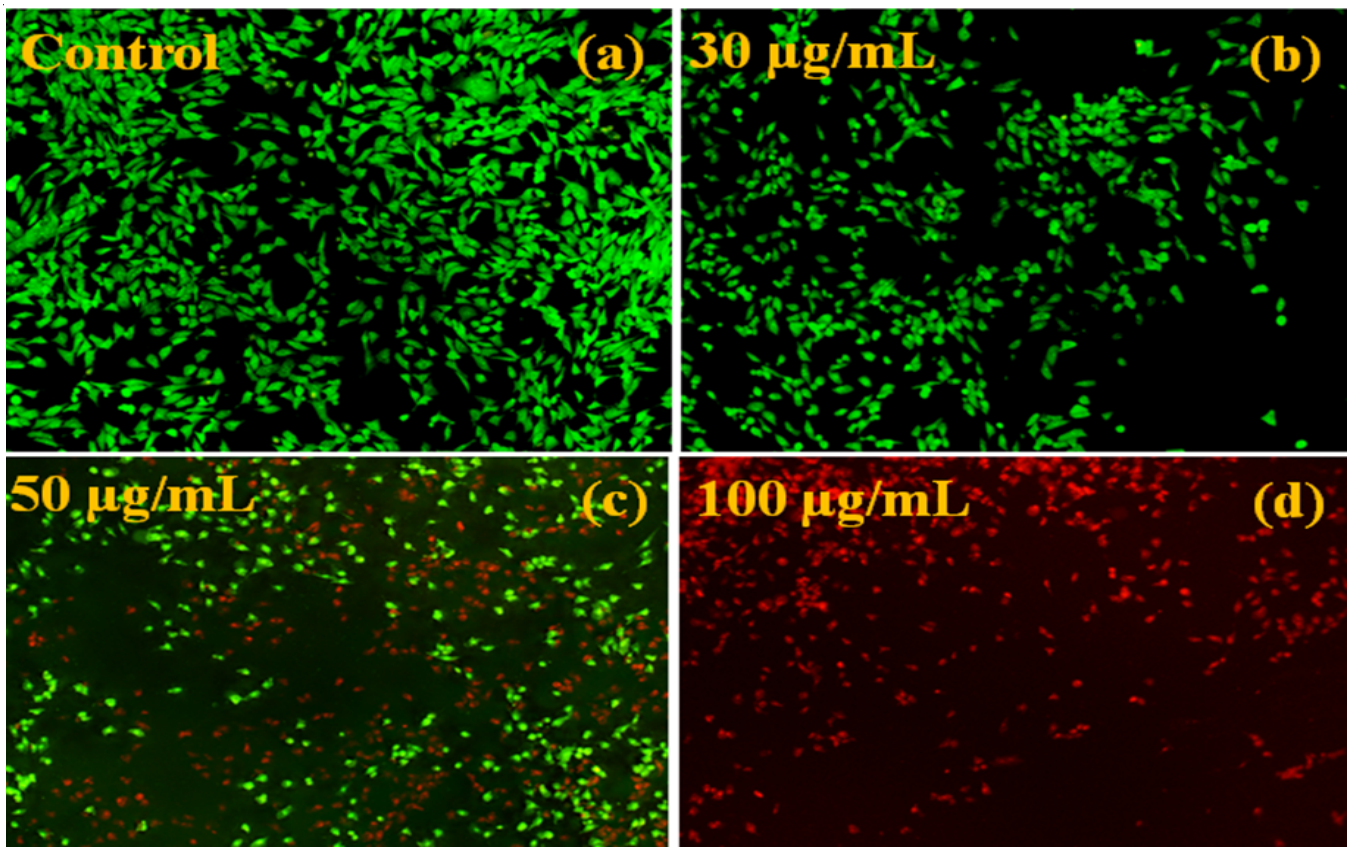

Fig. 8. Rh-123 staining in control cells indicates healthy mitochondria (high Δψm). LCF-HA treatment (30, 50 and 100 µg/mL) reduces Rh-123 uptake, suggesting mitochondrial dysfunction (low Δψm)

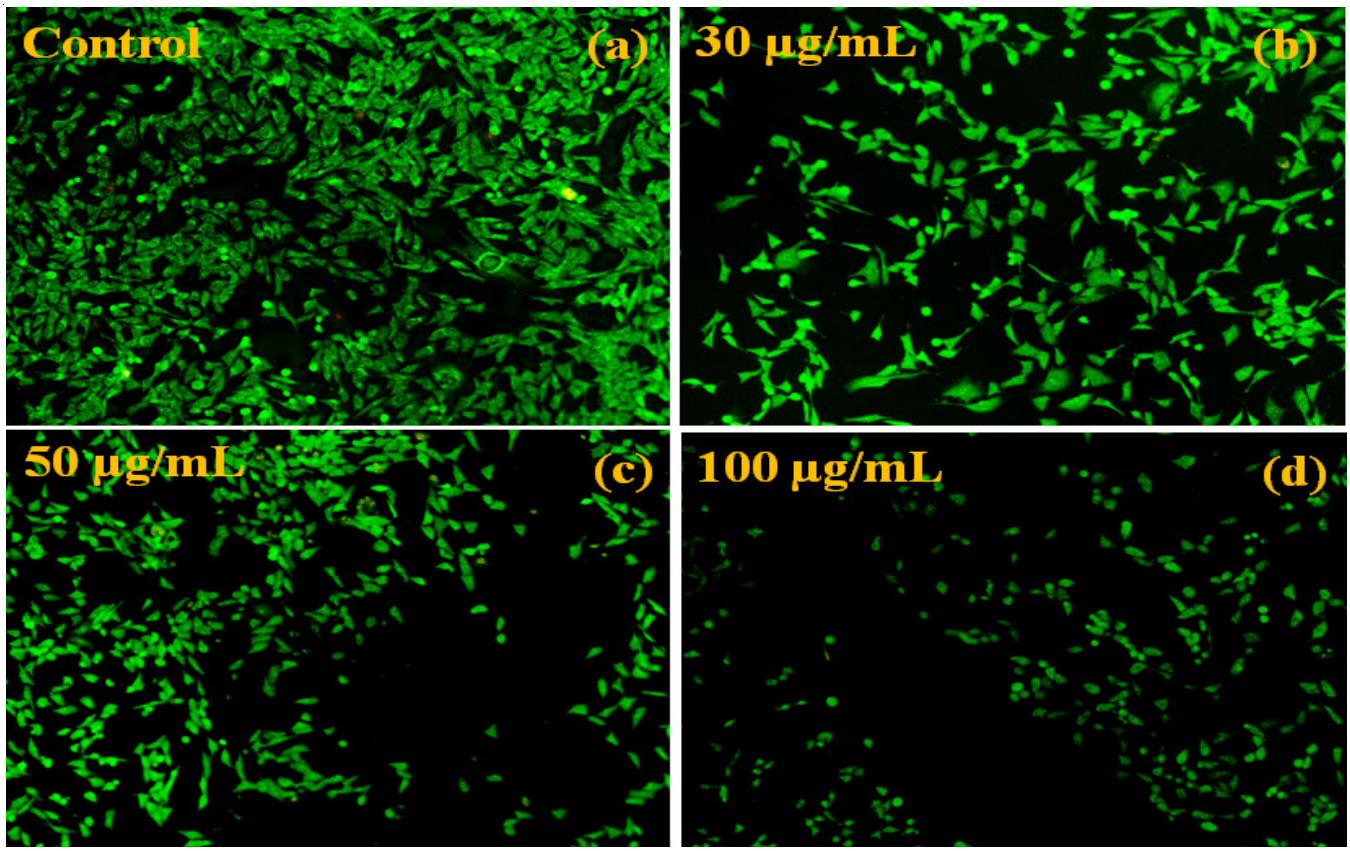

Fig. 9. LCF-HA induces apoptosis in osteosarcoma cells detected by AO/EB staining

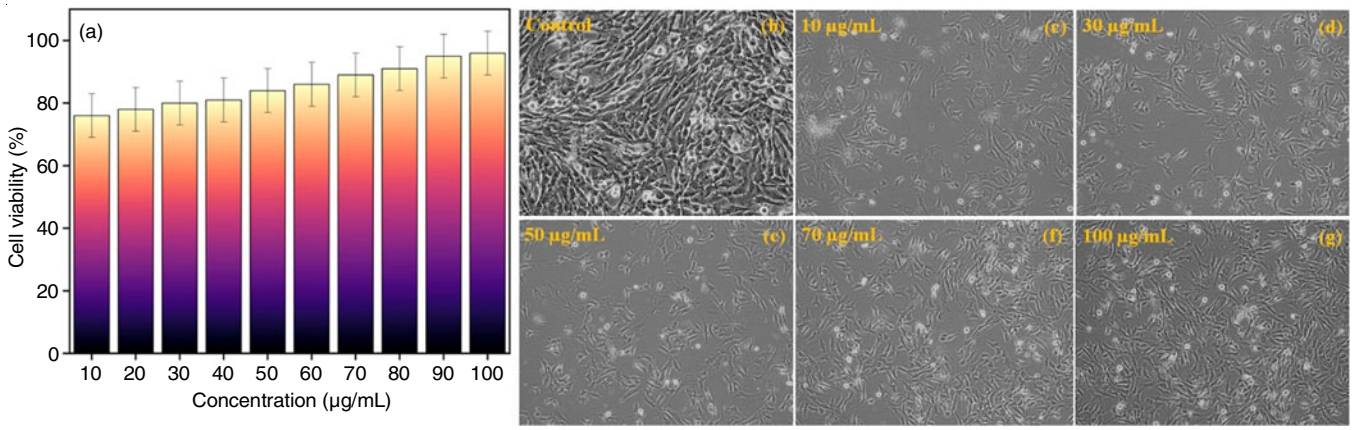

Fig. 10. Cell viability and microscope images of osteoblast cells on LCF-HA nanorods at different concentrations (n = 3)

Conclusion

This work emphasizes the significant potential of *Lantana camara* L. flower extract mediated hydroxyapatite (LCF-HA) nanorods for a combined treatment strategy targeting both cancer and bone infections. The green synthesis technique provides a cost-efficient, ecofriendly and easily expandable approach to prepare such nanorods with strong antibacterial properties, especially against Gram-positive bacteria linked to osteomyelitis, a bone infection. Moreover, the LCF-HA nanorods have a specific and destructive impact on osteosarcoma cells, which are cancerous bone tumour. The mechanism of action seems to include the initiation of apoptosis by generating reactive oxygen species (ROS) and interfering with the potential of the mitochondrial membrane. The dual impact of LCF-HA indicates its potential as an innovative therapeutic approach for managing osteosarcoma and avoiding osteomyelitis, a possible consequence that might occur during cancer therapy or owing to the weakened immune system of cancer patients. However, further *in vivo* investigations are necessary to confirm these results and evaluate the overall safety and effectiveness of LCF-HA for therapeutic use.

CONFLICT OF INTEREST

The authors declare that there is no conflict of interests regarding the publication of this article.

REFERENCES

1. K.S. Mohammad and S.A. Akhund, *Front. Biosci.*, **29**, 184 (2024); https://doi.org/10.31083/j.fbl2905184
2. S. Tsuzuki, S.H. Park, M.R. Eber, C.M. Peters and Y. Shiozawa, *Int. J. Urol.*, **23**, 825 (2016); https://doi.org/10.1111/iju.13170
3. A.K. Wani, A. Prakash, S. Sena, N. Akhtar, R. Singh, C. Chopra, E.E. Ariyanti, D. Mudiana, N.D. Yulia and F. Rahayu, *Crit. Rev. Oncol. Hematol.*, **196**, 104291 (2024); https://doi.org/10.1016/j.critrevonc.2024.104291
4. Y. Cao, H. Wang, S. Cao, Z. Liu and Y. Zhang, *Mater.*, **17**, 2584 (2024); https://doi.org/10.3390/ma17112584
5. S. Mondal, S. Park, J. Choi, T.T.H. Vu, V.H.M. Doan, T.T. Vo, B. Lee and J. Oh, *Adv. Colloid Interf. Sci.*, **321**, 103013 (2023); https://doi.org/10.1016/j.cis.2023.103013
6. M. Senthilkumar, S.K. Ramachandran, K.L. Servarayan, A. Periyasamy, V.V. Sivasamy and E. Sundaram, *Int. J. Biol. Sci.*, **2**, 133483 (2024); https://doi.org/10.1016/j.ijbiomac.2024.133483
7. R.H. Jacob, A.S. Afify, S.M. Shanab and E.A. Shalaby, *Biomass Convers. Biorefin.*, **14**, 2907 (2024); https://doi.org/10.1007/s13399-022-02333-3
8. B. Kumar, K. Smita and L. Cumbal, *J. Sol-Gel Sci. Technol.*, **78**, 285 (2016); https://doi.org/10.1007/s10971-015-3941-8
9. B.S. Surendra, C. Mallikarjunaswamy, S. Pramila and N.D. Rekha, *Environ. Nanotechnol. Monit. Manag.*, **15**, 100442 (2021); https://doi.org/10.1016/j.enmm.2021.100442
10. M. Rashtiani, E. Ghasemi, S. Hallajian and H. Ziyadi, *Inorg. Chem. Commun.*, **163**, 112361 (2024); https://doi.org/10.1016/j.inoche.2024.112361
11. S. Sarfi, E. Azaryan, M.Y. Hanafi-Bojd, F. Emadian Razavi and M. Naseri, *Sci. Rep.*, **14**, 14702 (2024); https://doi.org/10.1038/s41598-024-65582-4
12. A.F. Ali, Z.A. Alrowaili, E.M. El-Giar, M.M. Ahmed and A.M. El-Kady, *Ceram. Int.*, **47**, 3928 (2021); https://doi.org/10.1016/j.ceramint.2020.09.256
13. P.T.Y. Phi, T.T.N. Bich, P.T. Kien, N. Van Teo and P.P.X.N.Đ. Mo, *Vietnam J. Catal. Adsorpt.*, **13**, 99 (2024); https://doi.org/10.62239/jca.2024.017
14. G. Jing, M. Suhail, Y. Lu, B. Long, Y. Wu, J. Lu, J. Ge, M.Z. Iqbal and X. Kong, *ACS Biomater. Sci. Eng.*, **10**, 5068 (2024); https://doi.org/10.1021/acsbiomaterials.4c00277
15. S. Zuo, Q. Peng, T. Zhang, T. Luo, Y. Wang and Z. Peng, *Ceram. Int.*, **50**, 18105 (2024); https://doi.org/10.1016/j.ceramint.2024.02.251
16. M. Kawsar, M. Sahadat Hossain, S. Tabassum, N.M. Bahadur and S. Ahmed, *Nanoscale Adv.*, **6**, 2682 (2024); https://doi.org/10.1039/D3NA01122D
17. A. Mahanty and D. Shikha, *J. Mater. Res.*, **39**, 1128 (2024); https://doi.org/10.1557/s43578-024-01297-6
18. M. Zeng, Z. Xu, Z.Q. Song, J.X. Li, Z.W. Tang, S. Xiao and J. Wen, *World J. Orthop.*, **14**, 42 (2023); https://doi.org/10.5312/wjo.v14.i2.42
19. X. Huang, W. Wu, W. Yang, X. Qing and Z. Shao, *Colloids Surf. B Biointerfaces*, **190**, 110891 (2020); https://doi.org/10.1016/j.colsurfb.2020.110891
20. P. Yuan, Y. Min and Z. Zhao, *Biomater. Adv.*, **151**, 213466 (2023); https://doi.org/10.1016/j.bioadv.2023.213466
21. I. Lilienthal and N. Herold, *Int. J. Mol. Sci.*, **21**, 6885 (2020); https://doi.org/10.3390/ijms21186885
22. M. El-Garawani and S.E. Hassab, El-Nabi, *Can. J. Pure Appl. Sci.*, **10**, 3865 (2016).
23. K. Wang, Y. Ren, S. Lin, Y. Jing, C. Ma, J. Wang, X.B. Yuan, X. Han, H. Zhao, Z. Wang, M. Zheng, Y. Xiao, L. Chen, B.R. Olsen and J.Q. Feng, *Int. J. Biol. Sci.*, **17**, 2430 (2021); https://doi.org/10.7150/ijbs.61012